PROCEEDINGS OF SPIE

SPIEDigitalLibrary.org/conference-proceedings-of-spie

High-speed high-efficiency resonant-cavity-enhanced photodiodes

Ekmel Ozbay, Ibrahim Kimukin, Necmi Biyikli, Orhan Aytur, Mutlu Goekkavas, et al.

SPIE.

Invited Paper

High-Speed High-Efficiency Resonant Cavity Enhanced Photodiodes

Ekmel Ozbay[a], Ibrahim Kimukin[a], Necmi Bıyıklı[b] and Orhan Aytür[b],
Mutlu Gökkavas[c], Gökhan Ulu[c], and M. Selim Ünlü[c]
Richard P. Mirin[d], Kris A. Bertness[d], and David H. Christensen[d] , Elias Towe[e], and Gary Tuttle[f]

[a]Department of Physics, Bilkent University, Ankara, Turkey 06533
[b]Department of Electrical and Electronics Engineering, Bilkent University, Ankara, Turkey 06533
[c]Department of Electrical and Computer Engineering, Boston University, Boston MA 02215
[d]Optoelectronics Division, National Institute of Standards and Technology, Boulder CO 80303
[e]Department of Electrical Engineering, University of Virginia, Charlottesville, VA 2933
[f]Department of Electrical and Computer Engineering and Microelectronics Research Center, Iowa State University, Ames, IA 50011

ABSTRACT

In this paper, we review our research efforts on RCE high-speed high-efficiency p-i-n and Schottky photodiodes. Using a microwave compatible planar fabrication process, we have designed and fabricated GaAs based RCE photodiodes. For RCE Schottky photodiodes, we have achieved a peak quantum efficiency of 50% along with a 3-dB bandwidth of 100 GHz. The tunability of the detectors via a recess etch is also demonstrated. For p-i-n type photodiodes, we have fabricated and tested widely tunable devices with near 100% quantum efficiencies, along with a 3-dB bandwidth of 50 GHz. Both of these results correspond to the fastest RCE photodetectors published in scientific literature.

Keywords: high speed photodetectors, resonant cavity enhancement, Schottky diode, p-i-n photodiode, quantum efficiency

1. INTRODUCTION

As the information revolution continues at an increasing pace, there is an exponentially increasing demand for larger telecommunication bandwidths. The optical communication systems are currently the only viable solution for this bandwidth demand. Optoelectronic components such as semiconductor lasers, photodetectors, modulators, and optical amplifiers are at the heart of these communication systems, and the performance of all these devices should be increased to meet the existing and expected bandwidth requirements. Besides the optical communication systems, high-performance photodetectors are also vital components of optical measurement systems.[1] Both Schottky photodiodes,[2-4] and p-i-n photodiodes,[5,6] offer high-speed performance to fulfill the needs of such systems. However, the efficiency of these detectors has been typically limited to less than 10%, mostly due to the thin absorption region needed for short transit times. One can increase the absorption region thickness to achieve higher efficiencies, but this also means longer transit times that will degrade the high-speed performance of the devices. Resonant cavity enhanced (RCE) photodetectors offer the possibility of overcoming this limitation in the bandwidth-efficiency product of conventional photodetectors.[7-9] High-speed RCE photodetector research has mainly concentrated on using p-i-n photodiodes[10] and avalanche photodiodes, where 75% quantum efficiency along with a >20 GHz bandwidth[11], and 3 dB bandwidths as high as 33 GHz[12] have been reported. Recently, we have fabricated RCE Schottky photodiodes with 50% quantum efficiency and a 50 GHz frequency performance.[13,14] We have also achieved ~100 GHz performance, along with a 20% quantum efficiency.[15] Our work pin type RCE photodiodes resulted in >90% quantum efficiency along with a 50 GHz performance.[16] In this paper, we review our recent work on design, fabrication, and testing of widely tunable, high-speed RCE photodiodes for operation at 800-900 nm.

Part of the SPIE Conference on Photodetectors: Materials and Devices IV
San Jose, California • January 1999
SPIE Vol. 3629 • 0277-786X/99/$10.00

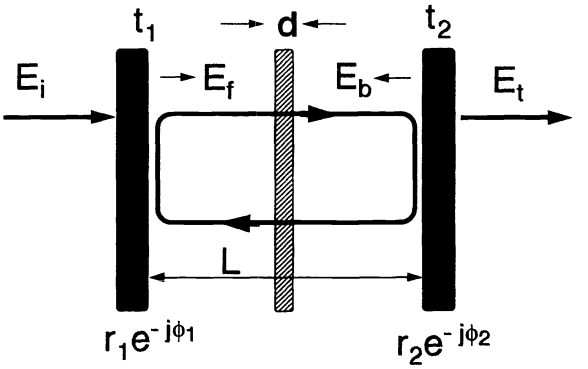

Figure 1. Schematics of the Fabry Perot cavity model. The shaded absorption region was used to simulate the active region placed in the cavity.

2. THEORY OF RESONANT CAVITY ENHANCEMENT IN PHOTODETECTORS

The well-known bandwidth-efficiency trade-off is a major blockade for using high-speed photodiodes in long-haul telecommunications. As the active region thickness is decreased to minimize the transit time for high-speed purposes, the quantum efficiency of the same device proportionally decreases. For a photodiode with transit-time limited frequency response, the 3-dB bandwidth can be formulated as

$$f_{3dB} \approx 0.45\frac{v}{d} \tag{1}$$

where v is the drift velocity of the charge carrier, and d is the active region thickness. For thin active regions, the absorption can be formulated as

$$\eta = (1-R)(1-e^{-\alpha d}) \approx (1-R)\alpha d \tag{2}$$

where α is the power absorption loss factor of the optical field within the active region, and $\alpha d \ll 1$ is assumed. Using equations 1 and 2, the bandwidth-efficiency product can be obtained as,

$$f_{3dB} \cdot \eta = 0.45(1-R)v\alpha \tag{3}$$

which is independent of the active region thickness.

This bandwidth-efficiency trade-off can be solved by placing the active region in a Fabry-Perot cavity (Figure1). This is usually achieved by integrating the photoactive region with a bottom Bragg mirror. In a Fabry-Perot cavity, the optical field is enhanced resulting in increased efficiencies. The electric field component for the forward traveling wave E_f inside the cavity (Figure 1) can be related to the incident field E_i as:

$$E_f = \frac{t_1}{1-r_1 r_2 e^{-\alpha d} e^{-j(2\beta L+\phi_1+\phi_2)}} E_i, \tag{4}$$

where $\mathbf{r_1 e^{-j\phi_1}}$ and $\mathbf{r_2 e^{-j\phi_2}}$ are the reflection coefficients of the mirrors, $\mathbf{t_1}$ is the transmission coefficient of the front mirror, β is the propagation constant for the traveling EM wave in air, and **L** is the total width of the cavity. The backward traveling wave E_b is related to E_f as:

$$E_b = r_2 e^{-\alpha d} e^{-j(\beta L+\phi_2)} E_f. \tag{5}$$

Using Eqs. (4) and (5), we can calculate the power enhancement factor η, which is defined as the ratio of the absorbed power inside the absorption layer, to the power of the incident EM wave,

$$\eta = \frac{(1+R_2 e^{-\alpha d})(1-R_1)}{1-2\sqrt{R_1 R_2}\, e^{-\alpha d}\cos(2\beta d+\phi_1+\phi_2)+R_1 R_2 e^{-\alpha d}} \tag{6}$$

where $\mathbf{R_1 = r_1^2}$ and $\mathbf{R_2 = r_2^2}$, are the reflectivities of the mirrors of the cavity. The above result is normalized with respect to the incident field absorbed by the detector in the absence of the cavity.

As can be seen from Equation 6, the introduction of a Fabry-Perot cavity can increase the quantum efficiency without effecting the high-speed properties. Besides, the detector becomes wavelength selective which may be very useful for wavelength division multiplexing (WDM) based optical communication systems.

3. RCE SCHOTTKY PHOTODIODES

3.1 DESIGN AND FABRICATION

We used an S-matrix method to design the epilayer structure of the RCE Schottky photodiodes. The structure was optimized for top-illumination and it consisted of a bottom Bragg mirror integrated with a Schottky diode structure. The mirror was formed by 15 pair AlAs(755 Å)/GaAs(637 Å) quarter wave stack designed to operate at 900 nm. The Schottky diode region had a 0.630 μm thick N^+ ($N_D = 3x10^{18}$ 1/cm^3) layer for ohmic contacts, and a 0.3 μm thick N^- ($N_D = 1.2 \times 10^{17}$ 1/cm^3) region for the generation and transport of photogenerated carriers. The N^- region consisted of a 1300 Å thick photoactive $In_{0.08}Ga_{0.92}As$ region, sandwiched between two GaAs N^- layers. The top GaAs N^- layer between the Schottky metal and the $In_{0.08}Ga_{0.92}As$ region had a thickness of 500 Å, while the other N^- region had a thickness of 1200 Å. The photoactive $In_{0.08}Ga_{0.92}As$ region was placed closer to the metal contact in order to equalize the transit times of photogenerated electrons and holes. The $In_{0.08}Ga_{0.92}As$/GaAs interfaces were graded to avoid hole-trapping. The total length of the cavity was designed to get the resonance to occur at 900 nm.

The epitaxial layers are grown by a solid-source MBE on semi-insulating GaAs substrates. The epitaxial design of the structure permits wavelength tuning by a recess etch of the top GaAs layer. Figure 2 shows the spectral reflectivity characteristics of the epitaxial wafer for different recess etches. As can be shown from the plot, the resonant wavelength can be tuned from 930 nm to 890 nm, by a 600 Angstrom recess etch.

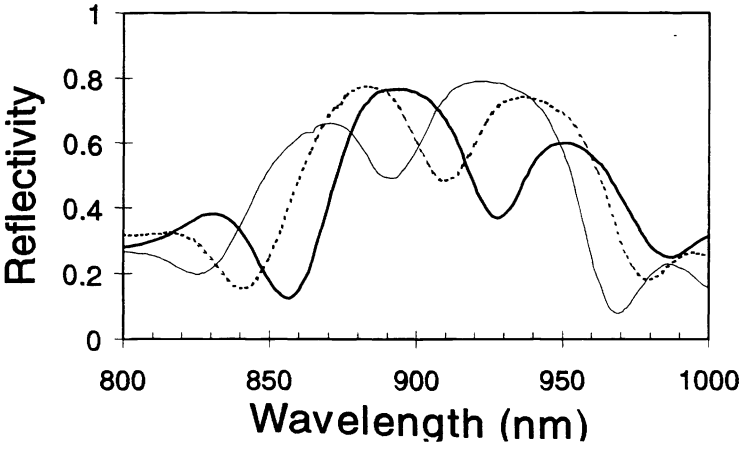

Figure 2. Reflectivities of the samples with different recess etches. The thick solid line refers to as grown sample, the dashed line refers to 300 Angstrom recess etched sample, and the thin solid line refers to the sample with a 600 Angstrom recess etch.

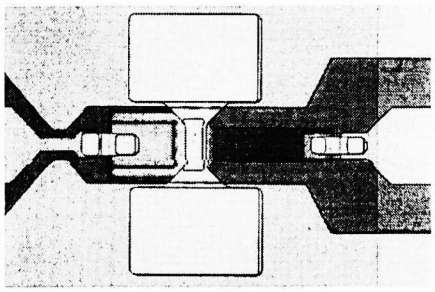

Figure 2. Microphotograph of the fabricated RCE photodiode.

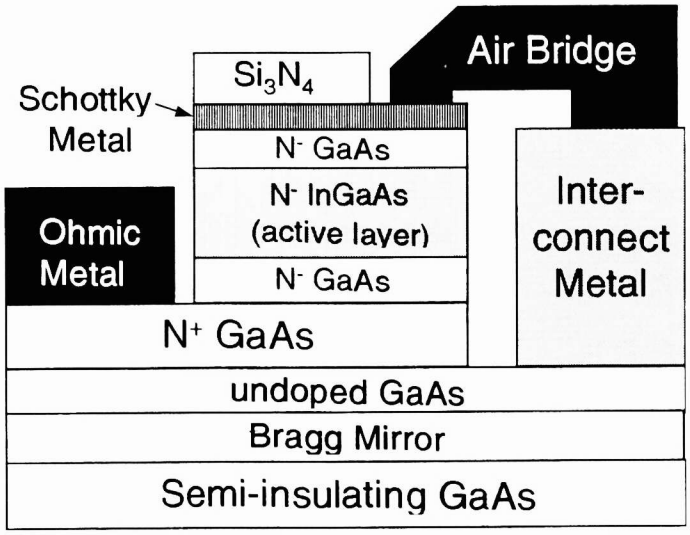

Figure 3. Diagram showing the cross section of a fabricated RCE Schottky photodiode.

We fabricated the epitaxial wafers using a monolithic microwave-compatible fabrication process. A microphotograph of the fabricated photodiodes is shown in Figure 2. First, ohmic contacts to the N+ layers were formed by a recess etch through the 0.3 micron N- layer. This was followed by a self-aligned Au-Ge-Ni liftoff and a rapid thermal anneal. The semi-transparent Schottky contact was formed by deposition of 200 Å Au. Using an isolation mask, we etched away all of the epilayers except the active areas. Then, we evaporated Ti/Au interconnect metal which formed coplanar waveguide (CPW) transmission lines on top of the semi-insulating substrate. The next step was the deposition and patterning of a 2000 Å thick silicon nitride layer. The thickness of the nitride layer was chosen to act as an antireflection coating for the RCE Schottky photodiode at the design wavelength. Besides passivation and protection of the surface, the nitride was also used as the dielectric of the metal-insulator-metal bias capacitors. Finally, 1.5 micron thick Au layer was used as an airbridge to connect the center of the CPW to the top Schottky metal. A cross-section of the fabricated photodiodes is shown in Figure 3. The resulting Schottky diodes had breakdown voltages larger than 12 V. The dark-current of a 150x150 μm device at -1V bias was 30 nA. Using the forward current-voltage characteristics, we measured the barrier height of the Schottky junction to be 0.83 eV.

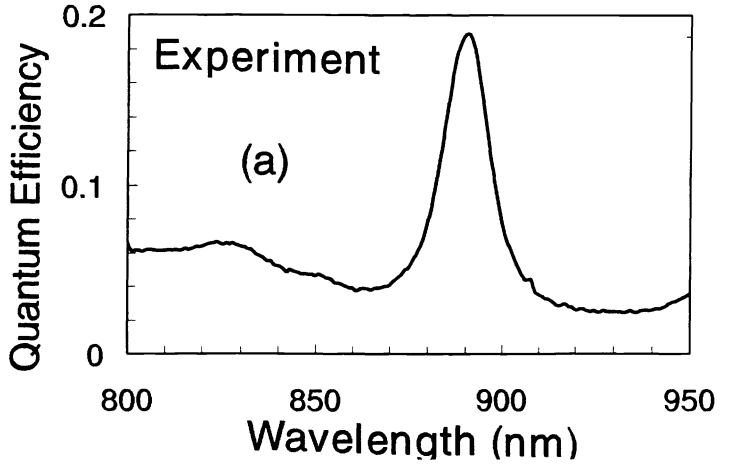

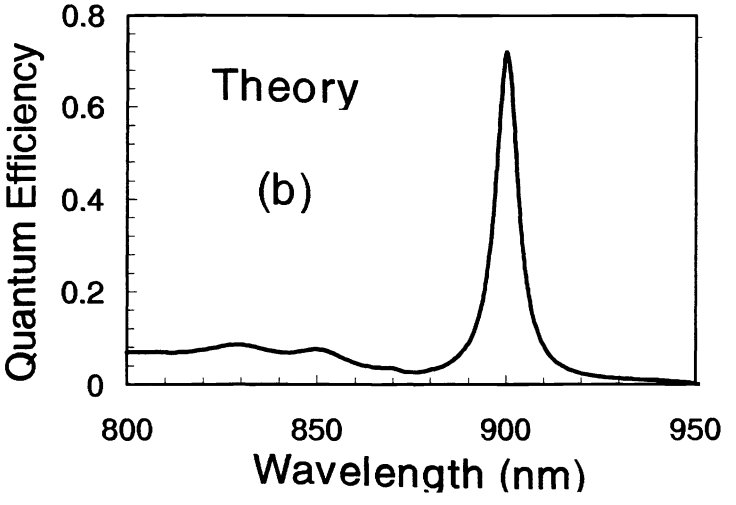

Figure 4. (a) Measured photoresponse of the RCE Schottky photodiode. (b) Simulated photoresponse of the same structure.

2.2 MEASUREMENTS

Photo response measurements were carried out in 700-900 nm wavelength range, by using a tungsten-halogen projection lamp as the light source, a single pass monochromator, a mechanical chopper, and a lock-in amplifier. Output of the monochromator was coupled to a multimode fiber. The monochromatic light was delivered to the devices by a lightwave fiber probe, and the electrical characterization was carried out on a probe station. The incident power spectrum was measured by a calibrated optical powermeter.

For spectral photoresponse measurements, we used a tungsten lamp source with a 1/3 meter grating monochromator. The monochromatic light was delivered to the devices by a multimode fiber and the electrical characterization was carried out on a probe station. The spectral response was corrected by measuring the light intensity at the fiber output by a calibrated optical power meter. Overall error is expected to be within several percent. For photospectral measurements, we used a 150x150 μm photodiode biased at -2.0 Volts.

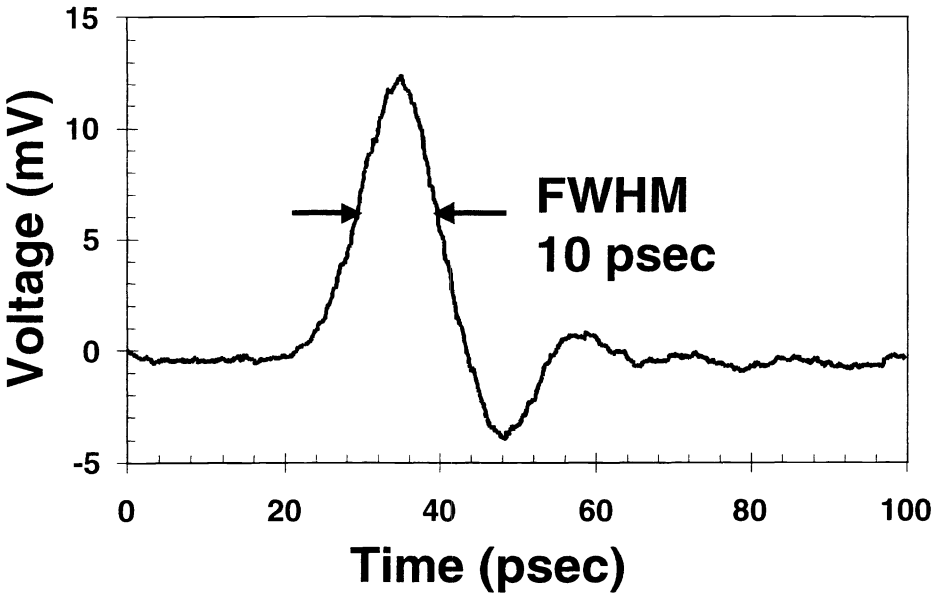

Figure 5. Pulse response of RCE Schottky photodiode.

The photoresponse of the device obtained by using the aforementioned set up is shown in Figure 4(a). For comparison purposes, the simulated quantum efficiency of the epitaxial structure is shown in Figure 4(b). There is a reasonable agreement between the calculated and the measured spectral responses. The resonant wavelength of the device is 895 nm, which is very close to the design wavelength of 900 nm. When compared with a single-pass structure, the enhancement factor of the device is in excess of 6 at the resonant wavelength. The full-width at half maximum was 15 nm, corresponding to a ~1.6% spectral width. Although we predicted a peak quantum efficiency of 70%, the measured peak quantum efficiency was around 18%. The discrepancy between the experiment and simulation is due to the shift of the Bragg mirror center wavelength during the MBE growth, which resulted in a 60% bottom mirror at 900 nm.

High-speed measurements were made with short optical pulses of 1.2 ps FWHM at 895 nm wavelength. The optical pulses from the laser were coupled into a single-mode fiber, and the other end of the fiber was brought in close proximity of the photodiode by means of a probe station. We used a 8x9 μm device biased at -2 Volts, and the photodiode output was measured by a 50 GHz sampling scope. Figure 5 shows the measured photodiode output which had a FWHM of 10 psec. There is no residual photocurrent after the pulse fall-time (except the smaller bumps due to reflections from the electrical contacts) which indicates that there is no diffusion component which may limit the bandwidth of the device. This is in accordance with our expectations, as the photoactive region is totally depleted, and the other regions are transparent at the resonant wavelength.[7] The measurement is limited by the experimental set-up. The pulsewidth of the 50 GHz scope, τ_{scope} is specified as 9.0 psec with an optimized Gaussian response. The optical pulse can also be assumed as a Gaussian pulse with a pulsewidth, $\tau_{optical}$, of 1.2 psec pulsewidth. The measured pulsewidth τ_{meas} can then approximated as:[17]

$$\tau_{meas} = \sqrt{\tau_{device}^{\,2} + \tau_{scope}^{\,2} + \tau_{optical}^{\,2}}. \qquad (7)$$

This is very accurate for Gaussian pulses and a good approximation for actual measurements. Using the above numbers in Eq. 7, the device speed is estimated to be around 4 psec. As our experimental result is very close to the measurement limit of the 50 GHz scope, we do expect a large uncertainty in this speed estimation. However, this estimated value (obtained from the experiment) value is in good agreement with our predicted device speeds. The device has an RC time constant of 1.4 psec, and the equalized electron and hole transit times are around 3.5 psec. The total speed of the device is then estimated to be 3.8 psec, which is very close to the value we obtain from Eq. 7.

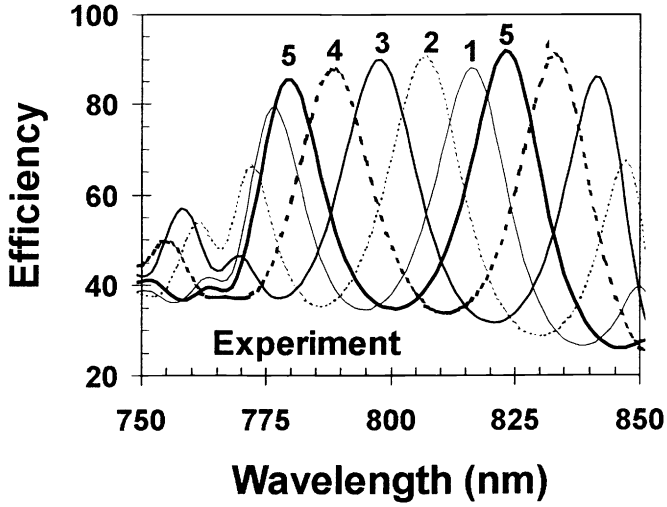

Figure 6. Experimental photoresponse characteristics of fabricated devices. Plot 1 corresponds to the as-grown sample, while plots 2-5 correspond to the characteristics after consecutive recess etches.

3. PIN PHOTODIODES

As mentioned earlier, p-i-n photodiodes are also widely used in telecommunication systems. The details of the p-i-n photodiode epitaxial structure we have used in this work is given in Ref. 16. In this structure, the bottom Bragg mirror is made of quarter-wave stacks ($Al_{0.20}Ga_{0.80}As/AlAs$) designed for high reflectance at 820 nm center wavelength. Carrier trapping was avoided by using linear composition grading at interfaces of the absorbing layer. The active layer thickness, d, was chosen such that the maximum quantum efficiency is obtained by,

$$R_1 = R_2 e^{-2\alpha d} \tag{8}$$

where α is the absorption coefficient, R_1 is the top air-semiconductor mirror reflectance, and R_2 is the bottom Bragg mirror reflectance [7]. The reflectivity measurements are used to investigate the epitaxial structure of the wafer. The resonance occurs at 826 nm with a measured reflectance minimum of 5%, while our theoretical simulations predict nearly zero reflectance at the same wavelength. The measured resonance wavelength changes from 826 nm at the center of the wafer, to 816 nm at the edge of the wafer. This epilayer thickness variation across the wafer and small deviations between growth and design explain the difference between the theoretical and experimental reflectance characteristics.

The samples were fabricated by a microwave-compatible process similar to the one used for the Schottky photodiodes. The p^+ ohmic contact was achieved by an Au/Ti liftoff. The n^+ and p^+ ohmic contacts were then achieved by a rapid thermal anneal at 450 °C for 25 seconds. The resulting p-i-n photodiodes had breakdown voltages greater than 14 V. The dark current of a 30 μm diameter circular device at –1 V bias was 20 pA.

Photoresponse measurements were carried out in the 750-850 nm wavelength range by using a tungsten-halogen projection lamp as the light source and a single pass monochromator. The output of the monochromator was coupled to a multimode fiber. The monochromatic light was delivered to the devices by a lightwave fiber probe, and the electrical characterization was carried out on a probe station. The spectral response was measured using a calibrated optical powermeter. For photospectral measurement, large area photodiodes (250 μm x 250 μm) were chosen to ensure all of the optical power is incident on the active area. The top p^+ layers were recess etched in small steps, and the tuning of the resonance wavelength within the Bragg mirror's upper and lower edges was observed. Figure 6(a) shows the spectral quantum efficiency measurements of a device obtained by consecutive recess etches. Plot 1 corresponds to the as-grown wafer, while plots 2, 3, 4, and 5 correspond to cumulative recess etches of 25, 50, 75, and 100 nm respectively. The peak experimental quantum efficiency (88%) of the as-grown sample at 816 nm increases to >90% values after the top absorbing GaAs cap layer is removed.

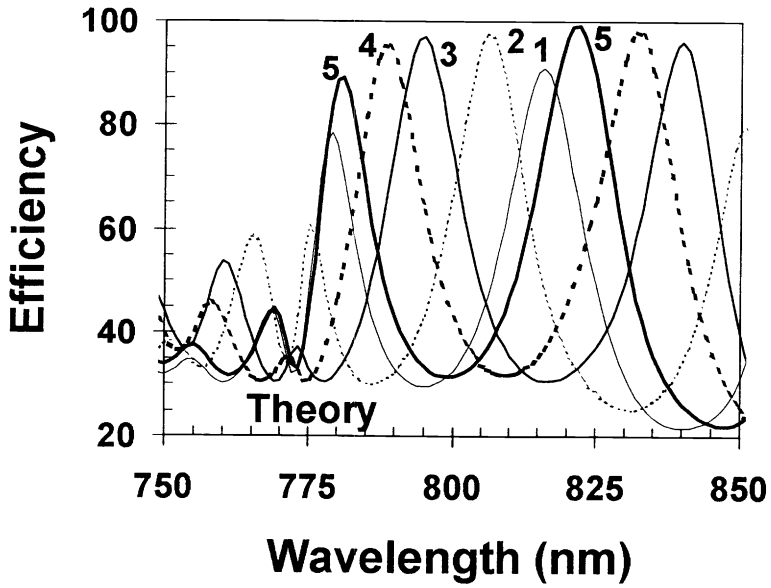

Figure 7. Theoretical photoresponse characteristics of fabricated devices. Plot 1 corresponds to the as-grown sample, while plots 2-5 correspond to the characteristics after consecutive recess etches.

The peak quantum efficiency remains almost constant with tuning until the resonance wavelength reaches to the lower edge of the Bragg mirror (780 nm). At this point, the second resonance appears around the upper edge of the Bragg mirror. The maximum measured quantum efficiency of 92% is obtained when the second resonance is tuned to 823 nm. As seen in Fig. 7(a), the resonance wavelength can be tuned for a total of 40 nm (835 nm to 795 nm) while keeping peak efficiencies above 90%. The peak efficiency is still above 85% for resonant wavelengths between 780-840 nm, corresponding to a tuning range of 60 nm. The full-width at half maximum (FWHM) of the devices is around 15 nm. The data shown in Fig. 7(a) are obtained at zero bias. The measured quantum efficiencies do not change at higher reverse biases, as the undoped active region is already depleted at zero bias. Figure 6(b) shows the transfer-matrix-method based theoretical simulations of the same recess etched structure. The theoretical peak quantum efficiencies are >95% for resonant wavelengths between 790-840 nm. The difference between the theoretical and experimental peak quantum efficiency values can be explained by the unaccounted for nonzero reflectance at the resonance wavelength, along with the 2% measurement error of the calibrated powermeter.

High-speed measurements were made with a picosecond Ti:Sapphire laser operating at 820 nm.[16] The 1.2 ps FWHM optical pulses from the laser were coupled into a single-mode fiber, and the other end of the fiber was placed in close proximity to a small area(7 μm x 13 μm) p-i-n photodiode by means of a probe station. The measured photodiode output has a 12 ps FWHM. The Fourier transform of the data has a 3 dB bandwidth of 38 GHz. The measured data are corrected by deconvolving the scope response, which is assumed to be a Gaussian pulse with a 7 ps rise time. After this correction, the device has a 3 dB bandwidth of 50 GHz. To the best of our knowledge, this is the highest frequency response reported for p-i-n type RCE photodiodes. We calculated the theoretical frequency response of the device as described in Ref. 10. The device under test has an RC time constant of 1.2 ps, corresponding to a 3 dB bandwidth of 230 GHz. The response of the device is mostly limited by the hole (7.5 ps) and electron (4.5 ps) transit times. Using these numerical values, we predict a 3 dB bandwidth of 50 GHz for the device under test, in good agreement with the deconvolved high-speed measurements. Our analysis reveals that the 3 dB bandwidth of the p-i-n structure can be further increased to >100 GHz by using a thinner active region. For that case a dielectric top Bragg mirror can be used to achieve >90% quantum efficiencies, which will yield a device with a bandwidth-efficiency product in excess of 100 GHz.

4. CONCLUSION

In summary, we reviewed our recent work on high-speed high-efficiency resonant cavity enhanced photodetectors. Using a microwave compatible planar fabrication process, we have designed and fabricated GaAs based RCE photodiodes. For RCE Schottky photodiodes, we have achieved a peak quantum efficiency of 50% along with a 3-dB bandwidth of 100 GHz. For p-i-n type photodiodes, we have fabricated and tested widely tunable devices with near 100% quantum efficiencies, along with a 3-dB bandwidth of 50 GHz. Both of these results correspond to the fastest RCE photodetectors published in scientific literature.

ACKNOWLEDGEMENTS

This work is supported by the Scientific and Technical Research Council of Turkey (TÜBİTAK) under contract No. 197-E044, in part by the Office of Naval Research under Grant N00014-96-10652, and in part by the National Science Foundation International Collaborative Research Program under Grant INT-9601770.

REFERENCES

1. J. E. Bowers and Y. G. Wey in *Handbook of Optics*, chap. 17, Michael Bass (ed.), McGraw-Hill, New York, (1995).
2. S. Y. Wang, and D. M. Bloom, Electron. Lett. **19**, pp. 554-555, 1983.
3. E. Özbay, K. D. Li, and D. M. Bloom, IEEE Photon. Technol. Lett. **3**, pp. 570-572, 1991.
4. K. D. Li, A. S. Hou, E. Özbay, and D. M. Bloom, Appl. Phys. Lett. **61**, pp. 3104-3106, 1992.
5. Y. G. Wey, M. Kamegawa, A. Mar, K. J. Williams, K. Giboney, D. L. Crawford, J. E. Bowers, and M. J. Rodwell, J. Lightwave Technol.**13**, pp. 1490-1494, 1995.
6. Y. G. Wey, K. S. Giboney, J.E. Bowers, M. J. W. Rodwell, P. Silvestre, P. Thiagarajan, and G.Y. Robinson, IEEE Photon. Technol. Lett. **5**, pp. 1310-1312, 1993.
7. M. S. Ünlü and S. Strite, J. Appl. Phys. Rev. **78**, pp. 607-628, 1995.
8. K. Kishino, M. S. Ünlü, J. I. Chyi, J. Reed, L. Arsenault, and H. Morkoç, IEEE J. Quantum Electron. **27**, pp. 2025-2031, 1991.
9. I. H. Tan, E. L. Hu, and J. E. Bowers, IEEE J. Quantum Electron. **31**, pp. 1863-1869, 1995.
10. C. C. Barron, C. J. Mahon, B. J. Thibeault, G. Wang, W. Jiang, L. A. Coldren, and J. E. Bowers, Electron. Lett. **30**, pp. 1796-1797, 1994.
11. H. Nie, K.A. Anselm, C. Hu, S. S. Murtaza, B.G. Streetman, and J.C. Campbell, Appl. Phys. Lett. **70**, pp. 161-163, 1997.
12. H. Nie, K.A. Anselm, C. Lennox, P. Yuan, C. Hu, G. Kinsey, B.G. Streetman, and J.C. Campbell, IEEE Photon. Tech. Lett. **10**, pp. 409-411, 1998.
13. E. Özbay, M. S. Islam, B. M. Onat, M. Gökkavas, O. Aytür, G. Tuttle, E. Towe, R. H. Henderson, and M. S. Ünlü, IEEE Photon. Technol. Lett. **9**, pp. 672-674, 1997.
14. M. S. Unlu, M. Gokkavas, B. M. Onat, E. Ata, E. Ozbay, R. P. Mirin, K. J. Knopp, K. A. Bertness, D. H. Christensen, Appl. Phys. Lett., volume **72,** pp. 2727-2729, 1998.
15. B. Onat, M. Gokkavas, E. Ozbay, E.P. Ata, E. Towe, and M.S. Unlu, Photonics Technology Letters **10**, pp. 707-709, 1998.
16. E. Ozbay, N. Bıyıklı, I. Kimukin, O. Aytür, M. Gökkavas, G. Ulu, R. Mirin, D. H. Christensen, and M. S. Ünlü, to appear in February 22, 1999 issue of Applied Physics Letters.
17. K. Rush, S. Draving, and J. Kerley, IEEE Spectrum **27**, pp. 38-39, 1990.